HHS Public Access

Author manuscript

Cell Rep. Author manuscript; available in PMC 2019 March 06.

Published in final edited form as:

Cell Rep. 2019 February 05; 26(6): 1389–1398.e3. doi:10.1016/j.celrep.2019.01.044.

Activation of the Rostral Intralaminar Thalamus Drives Reinforcement through Striatal Dopamine Release

Kara K. Cover[1], **Utsav Gyawali**[1], **Willa G. Kerkhoff**[1], **Mary H. Patton**[1], **Chaoqi Mu**[1], **Michael G. White**[1], **Ashley E. Marquardt**[1], **Bradley M. Roberts**[1], **Joseph F. Cheer**[2,3], and **Brian N. Mathur**[1,4,*]

[1]Department of Pharmacology, University of Maryland School of Medicine, Baltimore, MD 21201, USA

[2]Department of Anatomy and Neurobiology, University of Maryland School of Medicine, Baltimore, MD 21201, USA

[3]Department of Psychiatry, University of Maryland School of Medicine, Baltimore, MD 21201, USA

[4]Lead Contact

SUMMARY

Glutamatergic projections of the thalamic rostral intralaminar nuclei of the thalamus (rILN) innervate the dorsal striatum (DS) and are implicated in dopamine (DA)-dependent incubation of drug seeking. However, the mechanism by which rILN signaling modulates reward seeking and striatal DA release is unknown. We find that activation of rILN inputs to the DS drives cholinergic interneuron burst-firing behavior and DA D2 receptor-dependent post-burst pauses in cholinergic interneuron firing. *In vivo*, optogenetic activation of this pathway drives reinforcement in a DA D1 receptor-dependent manner, and chemogenetic suppression of the rILN reduces dopaminergic nigrostriatal terminal activity as measured by fiber photometry. Altogether, these data provide evidence that the rILN activates striatal cholinergic interneurons to enhance the pursuit of reward through local striatal DA release and introduce an additional level of complexity in our understanding of striatal DA signaling.

Graphical Abstract

*Correspondence: bmathur@som.umaryland.edu.

AUTHOR CONTRIBUTIONS

K. K.C. and B.N.M. conceived the experiments. K.K.C., U.G., W.G.K., M.H.P., C.M., M.G.W., A.E.M., B.M.R., and B.N.M. performed the experiments. J.F.C. provided material and technical support. K.K.C. and B.N.M. wrote the manuscript.

SUPPLEMENTAL INFORMATION

Supplemental Information includes three figures and can be found with this article online at https://doi.org/10.1016/j.celrep.2019.01.044.

DECLARATION OF INTERESTS

The authors declare no competing interests.

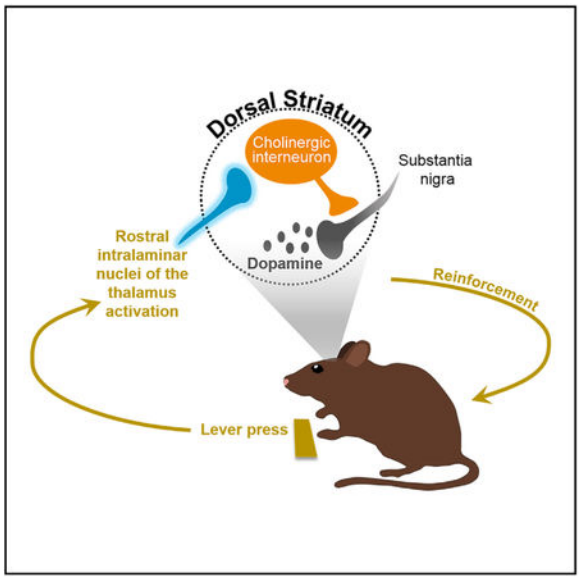

In Brief

Cover et al. identify a glutamatergic thalamostriatal pathway that locally elicits striatal dopamine release to drive reward-related behavior in mice.

INTRODUCTION

Dopamine (DA) release in the dorsal striatum (DS) is a critical component of reinforcement (Bamford et al., 2018). Midbrain DA neuron phasic firing correlates with discrepancies between reward expectation and outcome and is hypothesized to facilitate reinforcement learning, as described by the reward prediction error model (Schultz, 2001). Single-unit recordings in the area of the midbrain that projects to the DS, the substantia nigra pars compacta, reveal DA neuron burst firing that corresponds with the start and stop of action sequences (Jin and Costa, 2010), as well as movement kinematics (Barter et al., 2015; Fan et al., 2012).

At the level of the DA neuron terminal field in the DS, parallel phasic changes in DA release relate to reward and action execution (Howard et al., 2017; Howe and Dombeck, 2016; Roitman et al., 2004). Diverging from DA neuron somatic activity, however, phasic increases in DA release correlate with reward anticipation (Hamid et al., 2016). Moreover, striatal DA release ramps up as a function of spatial proximity to a reward and scales to changes in the length of a maze that is required to be traversed to obtain a reward (Howe et al., 2013). Whereas DA neuron firing rates ramp up only when reward reinforcement is uncertain (Fiorillo et al., 2003), increases in DA release persists in sessions in which reward is guaranteed (Howe et al., 2013). Altogether, these accounts of diverse activity across DA neuron soma and axon terminals suggest the existence of behaviorally relevant DA release mechanisms acting at the level of the DA neuron terminal field (Berke, 2018).

Supporting this notion, electrical stimulation of non-selective thalamic inputs to the striatum drives cholinergic interneurons to burst fire and subsequently pause their firing in a DA D2 receptor-dependent manner (Ding et al., 2010). Because this so-called burst-pause activity of cholinergic neurons is associated with learning (Aosaki et al., 1994), these data collectively suggest that the intralaminar nuclei of the thalamus may direct cholinergic interneuron activity *in vivo* to shape action learning through local striatal DA release mechanisms (Zhang et al., 2018). DA release is observed in both the dorsal and the ventral striatum following synchronous cholinergic interneuron activation (Cachope et al., 2012; Mateo et al., 2017; Threlfell et al., 2012). Because of the innervation of cholinergic interneurons by the parafascicular thalamic intralaminar nucleus (Pf), activation of this structure elicits local striatal DA release in a nicotinic acetylcholine receptor-dependent manner (Threlfell et al., 2012).

In addition to the Pf, the rostral intralaminar nuclei of the thalamus (rILN), consisting of the tightly bundled central lateral, paracentral, and central medial nuclei, similarly projects to the striatum (Berendse and Groenewegen, 1990; Hunnicutt et al., 2016). This raises the possibility that rILN activity may influence striatal DA release. rILN projections to the DS facilitate incubation of methamphetamine craving in a DA D1 receptor-dependent manner (Li et al., 2018). Here, we find that rILN terminal activation in DS slices drives DA-dependent cholinergic interneuron burst-pause activity and, accordingly, evokes DS DA release in an acetylcho-line-dependent manner. *In vivo*, we report that suppressing rILN activity modulates dopaminergic nigrostriatal terminal activity and that optogenetic stimulation of rILN terminals facilitates intracranial self-stimulation in a D1 receptor-dependent manner. We also present evidence that cholinergic interneurons contribute to this behavior. These results underscore the potential for non-canonical, local striatal release mechanisms in mediating reward-related behaviors.

RESULTS

The rILN Elicits Local Striatal DA Release through Cholinergic Interneurons

To determine whether rILN activation elicits striatal DA release through a cholinergic interneuron-dependent mechanism, we first explored whether rILN terminals innervate cholinergic interneurons in the DS. We expressed channelrhodopsin (ChR2)-enhanced yellow fluorescent protein (eYFP) in the rILN (Figure S1) and optogenetically activated ChR2-expressing rILN terminals while recording from cholinergic interneurons using whole-cell patch-clamp electrophysiology (Figures 1A–1D). We observed characteristic tonic firing in tdTomato-labeled neurons (Figure 1E). Activation of rILN terminals with single blue light pulses evoked post-synaptic currents evoked by optogenetic activation (oPSCs) that were abolished in the presence of AMPA and NMDA receptor antagonists, NBQX and AP5, respectively ($t(8) = 8.56$, $p < 0.0001$) (Figure 1F).

To examine whether rILN afferents in the DS sufficiently innervate cholinergic interneurons to elicit burst action potential firing followed by the characteristic DA-dependent pause in firing behavior (Ding et al., 2010), we recorded from cholinergic interneurons in current-clamp mode while optogenetically activating rILN afferents. We found that a 1.5 s light pulse train induced a burst-pause firing response in cholinergic interneurons (Figure 1G).

The time to first action potential following the burst response was significantly greater than the pre-burst interspike interval (ISI) ($p = 0.001$) (Figure 1H). To determine whether the post-burst pause was DA mediated, we applied the D2 receptor antagonist sulpiride (Figure 1I). Sulpiride produced a trending, but not significant, increase in the baseline firing rate ($p = 0.11$) (Figure 1J) but no difference in burst response ($p = 0.85$) (Figure 1K) compared with control recordings. Sulpiride incubation significantly shortened the post-burst pause in firing ($p = 0.005$) (Figure 1L) and decreased the post-burst ISI to the baseline ISI ratio ($p = 0.028$) (Figure 1M).

The DA-modulated burst-pause firing behavior we observed in striatal slice suggests that rILN afferent activation leads to local DA release. To provide direct evidence of this, we used fast-scan cyclic voltammetry (FSCV) to measure electrical currents derived from DA transients. Optogenetic activation of rILN terminals in acute striatal slices evoked transient DA release in the DS (Figures 2A and 2B). DA release persisted across repeated light pulses, decaying to an average 73.7% ± 7.1% of baseline ($t(7) = 3.69$, $p = 0.0078$) and was eliminated by NBQX (compared to control recordings: $t(14) = 9.86$, $p < 0.0001$; compared to NBQX baseline: $t(7) = 64.69$, $p < 0.0001$) (Figure 2C), but not by AP5, of which current decayed to 79.0% ± 7.3% of baseline (compared to control: $t(14) = 0.52$, $p = 0.61$; compared to AP5 baseline: $t(7) = 2.87$, $p = 0.02$) (Figure 2D). The nicotinic receptor antagonist mecamylamine also abolished optogenetically evoked DA release (compared to control: $t(14) = 10.31$, $p < 0.0001$; compared to mecamylamine baseline: $t(7) = 1009$, $p < 0.0001$) (Figure 2E). To confirm that the recorded current was DA derived, and not serotonin, for example, we applied the D2 receptor agonist quinpirole to activate DA autoreceptors. Quinpirole significantly attenuated the light-evoked current compared to the control condition ($t(13) = 9.61$, $p < 0.0001$) (Figure 2F).

rILN Activity Modulation of Nigrostriatal Terminal Activity and Movement

Because rILN terminal activation robustly elicits local DA release, we next sought to determine whether the rILN provides an ongoing modulation of dopaminergic nigrostriatal terminal activity *in vivo*. To this end, we employed fiber photometry to monitor nigrostriatal terminal activity (Parker et al., 2016) while chemogenetically suppressing rILN activity. To first validate the efficacy of inhibitory DREADD receptor hM4Di-mediated suppression of glutamate release from rILN into the DS, we co-expressed ChR2-eYFP and hM4Di-mCherry in the rILN and recorded oPSC events in medium spiny neurons (MSNs) in acute striatal slices (Figure 3A). Activating hM4Di receptors with clozapine-N-oxide (CNO) reduced oPSC amplitude to 44.5% ± 5.2% of baseline compared to control artificial cerebral spinal fluid (aCSF) with an amplitude of 98.4% ± 11.7% ($t(13) = 3.57$, $p = 0.0034$; compared to CNO baseline: $t(5) = 10.60$, $p = 0.0001$) (Figure 3B).

We next used fiber photometry to monitor population-level, activity-dependent calcium transients arising from GCaMP6f-expressing dopaminergic nigrostriatal terminals in mice. These mice also expressed either hM4Di-mCherry or mCherry fluorophore alone in the rILN and were unilaterally implanted with a multimode fiber in the DS (Figure 3C). CNO administration significantly reduced the GCaMP6f peak signal in hM4Di-expressing mice, but not mCherry-expressing mice, compared with vehicle in freely moving mice (Figures 3D

and 3E). Two-way ANOVA showed main effects for the drug ($F_{1,28}$ = 11.53, p = 0.0021), the animal group ($F_{-1,28}$ = 5.78, p = 0.023), and a significant interaction ($F_{-1,28}$ = 5.78, p = 0.023) of the two factors. The off-peak spectral channel photon count, which is subtracted from the GCaMP6f-associated channel to derive the peak signal, did not differ significantly before or after CNO administration in either group (group: $F_{1,27}$ = 1.618, p = 0.214; drug: $F_{1,27}$ = 3.42, p = 0.076; interaction: $F_{1,27}$ = 3.48, p = 0.073). The change in nigrostriatal activity-dependent calcium activity was accompanied by significant reductions in movement in hM4Di-expressing mice, but not mCherry-expressing mice, as measured by total distance moved (drug: $F_{1,28}$ = 2.95, p = 0.097; group: $F_{1,28}$ = 2.87, p = 0.095; interaction: $F_{1,28}$ = 11.12, p = 0.0024) (Figure 3F), maximum velocity achieved (drug: $F_{1,28}$ = 2.13, p = 0.16; group: $F_{1,28}$ = 0.62, p = 0.44; interaction: $F_{1,28}$ = 8.15, p = 0.008) (Figure 3G), and percentage of time in motion (drug: $F_{1,28}$ = 2.66, p = 0.11; group: $F_{1,28}$ = 5.62, p = 0.025; interaction: $F_{1,28}$ = 8.99, p = 0.0057) (Figure 3H) during a 5 min period.

rILN → DS Pathway Activation Is Behaviorally Reinforcing

Because DS DA is associated with behavioral reinforcement (Faure et al., 2005; Robinson et al., 2007), we next investigated whether activation of rILN inputs into the DS supports reinforcement in a DA-dependent manner. To test this, we trained mice in an optical intracranial self-stimulation (oICSS) paradigm (Figure 4A). Mice expressing ChR2-eYFP in the rILN lever pressed for light activation of rILN → DS terminals significantly more than the non-reinforced lever and reliably switched lever preference when light delivery was reversed to the opposite lever 24 h later (Figure 4B). Because rILN-dependent incubation of drug craving is mediated by DS DA D1 receptors (Li et al., 2018), we investigated whether D1 receptor activity was necessary for oICSS. We found that administration of the D1 receptor antagonist SCH23390 before oICSS sessions significantly reduced this preference for the light-paired lever, as did sessions in which neither lever was paired with light delivery. Within-subject two-way ANOVA showed a main effect of the lever on day 2 ($F_{1,8}$ = 54.41, p < 0.0001), not day 1 ($F_{1,8}$ = 4.12, p = 0.077); main effects for the condition (day 1: $F_{3,24}$ = 6.24, p = 0.003; day 2: $F_{3,24}$ = 9.96, p = 0.0002); and significant interactions (day 1: $F_{3,24}$ = 14.02, p < 0.0001; day 2: $F_{3,24}$ = 20.90, p < 0.0001). In contrast, mice expressing eYFP alone in the rILN did not demonstrate a preference for the light-paired lever (Figure 4C). Analysis of the lever and condition showed the main effects for the lever (day 1: $F_{1,8}$ = 9.17, p = 0.016; day 2: $F_{1,8}$ = 12.74, p = 0.007); the main effect of the condition for day 2 ($F_{3,24}$ = 5.60, p = 0.005), not day 1 ($F_{3,24}$ = 1.84, p = 0.167); and no significant interaction between the two factors for either day (day 1: $F_{3,24}$ = 1.156, p = 0.347; day 2: $F_{3,24}$ = 0.227, p = 0.877). Assessing the effect of light delivery and drug administration on total press rates, ChR2-eYFP mice pressed significantly more during light-reinforced sessions following vehicle administration (Veh+Light) than in any other condition, whereas eYFP mice demonstrated no significant differences in total press rates between the conditions (Figure S2). Moreover, total press rates between the two animal groups only differed significantly in the Veh+Light condition. Significant effects were found in the condition (day 1: $F_{3,48}$ = 7.8, p = 0.0003; day 2: $F_{3,48}$ = 14.6, p < 0.0001), the animal group (day 1: $F_{1,16}$ = 3.0, p = 0.102; day 2: $F_{1,16}$ = 14.4, p = 0.0016), and an interaction of the two factors (day 1: $F_{3,48}$ = 7.8, p < 0.001; day 2: $F_{3,48}$ = 4.06, p = 0.012).

Because the rILN projects to MSNs (Ellender et al., 2013), we next examined whether the rILN → cholinergic interneuron circuit is required for rILN-evoked behavioral reinforcement by ablating cholinergic interneurons at the site of light delivery with a viral taCasp3 construct (Figure 4D). Compared to a control cohort of mice injected with DIO-mCherry in the striatum, taCasp3 mice failed to demonstrate a preference for the light-paired lever on the first test day (lever: $F_{1,11} = 10.14$, $p = 0.0087$; animal group: $F_{1,11} = 0.62$, $p = 0.45$; interaction: $F_{1,11} = 5.61$, $p = 0.037$) (Figure 4E, left). Upon lever reversal, however, taCasp3 mice performed similarly to mCherry controls by pressing the light-paired lever significantly more than the non-reinforced lever (lever: $F_{1,11} = 37.15$, $p < 0.0001$; animal group: $F_{1,11} = 0.81$, $p = 0.39$; interaction: $F_{1,11} = 0.67$, $p = 0.43$) (Figure 4E, right).

Pf → DS Pathway Activation Evokes a Transient DA Response

To understand how rILN-evoked striatal DA release and behavior compare with those of Pf inputs, we injected ChR2-eYFP in the Pf. We found that optogenetic activation of Pf terminals evoked DS DA release (Figures S3A and S3B), confirming findings by Threlfell et al. (2012). This DA response decayed significantly over time compared to rILN-evoked release (Figure S3C). Analyzing evoked current normalized to the first time point, there were significant main effects of time ($F_{9,198} = 25.88$, $p < 0.0001$) and thalamic region ($F_{1,22} = 36.42$, $p < 0.0001$), with a significant interaction ($F_{9,198} = 9.61$, $p < 0.0001$). Pf-evoked DA release was attenuated by mecamylamine compared to control ($t(11) = 4.39$, $p = 0.0011$) (Figure S3D) (Threlfell et al., 2012). We then assessed whether Pf-evoked DA release is behaviorally reinforcing. Mice expressing ChR2-eYFP in Pf did not prefer to press the lever paired with bilateral DS light delivery on the first test day compared to the non-reinforced lever. Although mice pressed the light-paired lever more upon lever reversal on day 2 (Figure S3E), two-way ANOVA did not reveal main effects for the lever ($F_{1,6} = 1.35$, $p = 0.29$), the day ($F_{1,6} = 1.28$, $p = 0.30$), or an interaction of the two factors ($F_{1,6} = 4.82$, $p = 0.07$).

DISCUSSION

These data support the notion that the rILN → DS pathway activates cholinergic interneurons to drive local DA release from nigrostriatal terminals and that activity of this thalamostriatal pathway is associated with nigrostriatal terminal activity *in vivo*. These data show that local striatal DA release is sufficient to support behavioral reinforcement.

Although the rILN has not been studied in depth, Li et al. (2018) demonstrated rILN → DS-mediated incubation of drug seeking that supports a role for this thalamic region in reward-related behavior. Given that the rILN is innervated by sensory processing structures (Van der Werf et al., 2002), this pathway may relay salient sensory cues to inform actions. Furthermore, specific rILN → DS projections are linked to movement kinematics (Chen et al., 2014), as well as behavioral flexibility and attentional set shifting (Kato et al., 2018). Altogether, the Pf and rILN likely act in concert to shape striatal DA signals and thus mediate an action response to reward-related cues.

Our finding that cholinergic interneuron ablation disrupted behavioral reinforcement on the first test day suggests that rILN-evoked behaviors may be mediated through the combination

of rILN synapses on other striatal cell populations to facilitate the behavioral reinforcement observed on the second test day. Alternatively, the day 2 lever-pressing effect may arise from plastic changes at rILN → MSN synapses that developed in the absence of cholinergic interneurons. Future work is necessary to determine the possible contribution of rILN → MSN synapses in supporting behavioral reinforcement in a DA- and acetylcholine-independent manner.

A comparison of rILN and Pf projections to DS suggests that they have distinct axon morphology, axo-dendritic connections (Lacey et al., 2007), and plasticity mechanisms (Ellender et al., 2013). Together with possible activation of the presynaptic mGluR2/3 and D2 autoreceptors on thalamic and nigrostriatal afferents, respectively, rILN projections may uniquely synapse on cholinergic interneurons to support the observed differences in DA release compared to Pf afferents. Mice exhibited a preference (although not a significant one) for Pf stimulation upon lever reversal on day 2, which is reminiscent of Pf → cholinergic interneuron pathway-mediated reversal learning (Bradfield et al., 2013).

Combined with potential cholinergic interneuron → nigrostriatal terminal and Pf → cholinergic interneuron → nigrostriatal terminal pathways, our presently described rILN → cholinergic interneuron → nigrostriatal terminal circuit reveals another possible local DS DA release pathway. This suggests that somatic activity is only one contributor to DA release and approaches that exclusively examine this dimension may not fully capture the dynamic signaling occurring at the striatal level that guides behavior (Berke, 2018). Nigrostriatal axons extensively arborize; a single neuron gives rise to an estimated 1 million synapses (Matsuda et al., 2009; Pissadaki and Bolam, 2013). Local axo-axonic circuits may thus provide more spatially restricted DA signaling that may be driven by associative thalamic structures encoding salient sensory information. Cortical afferent stimulation also evokes DA release in striatal slices through cholinergic interneuron activation (Kosillo et al., 2016; Mateo et al., 2017), which further suggests that axo-axonic synapses for local DS DA release are a recurring theme. These synaptic configurations are frequently observed in electron microscopy studies, including in the DS(Soghomonian et al., 1989).

The expanse of pathologies involving DA dysfunction potentially implicate the rILN → DS circuit in various neuropsychiatric disorders. The degeneration of the nigrostriatal pathway in Parkinson’s disease is associated not only with motor dysfunction (Wichmann and DeLong, 2003) but also motivational deficits (Renfroe et al., 2016) and cognitive deficits (Hanganu et al., 2015). Degeneration of thalamostriatal projections is reported in Parkinson’s disease (Halliday, 2009; Smith et al., 2014), which suggests that loss of rILN → DS-mediated DA signaling may contribute to disease symptomology (Melief et al., 2018). Furthermore, aberrant DS DA transmission is implicated in both attention deficit/hyperactivity disorder (del Campo et al., 2013; Volkow et al., 2007a) and drug abuse (Volkow et al., 2007b). Investigating how the rILN → DS circuit contributes to these disease states stands to reveal targets for therapeutic intervention.

STAR★METHODS

Detailed methods are provided in the online version of this paper and include the following:

CONTACT FOR REAGENT AND RESOURCE SHARING

Further information and requests for resources and reagents should be directed to and will be fulfilled by the Lead Contact, Brian Mathur (bmathur@som.umaryland.edu).

EXPERIMENTAL MODEL AND SUBJECT DETAILS

2-4-month-old male and female C57BL/6J (wild-type) mice were given *ad libitum* access to food and water and maintained on a 12:12 h light/dark cycle (lights on at 0700 hr). Mice were housed with littermates (2-5 per cage), except for those singly-housed following fiber implantation. To visually-identify cholinergic interneurons for electrophysiological recordings, ChAT-IRES-Cre mice were crossed in-house with tdTomato reporter mice (Ai9(RCL-tdT) to selectively express tdTomato fluorophore in Cre-recombinase-expressing cholinergic neurons (referred here as "ChAT-tdT"). Heterozygous DAT-IRES-Cre mice (DAT-cre) were used for *in vivo* photometry. All experiments were performed in accordance with the United States Public Health Service Guide for Care and Use of Laboratory and were approved by the Institutional Animal Care and Use Committee at the University of Maryland, Baltimore.

METHOD DETAILS

Surgical Procedures—To virally express ChR2 in the rILN, wild-type mice were stereotaxically injected under isoflurane (5% induction, 1%–2% maintenance) with AAV-hSyn-ChR2-eYFP or control AAV-hSyn-eYFP viruses (See Figure S1). Viruses were injected at a volume of 300 nl/side and rate of 20 nl/min in the rILN (relative to bregma in mm, anterior-posterior (AP) −1.4, medial-lateral (ML) ± 0.35, dorsalventral (DV) −3.55) or Pf (250 nL/side; AP −2.5, ML ± 0.75, DV −3.25) with a 25G syringe (Hamilton Company). To virally ablate striatal cholinergic interneurons, AAV5-flex-taCasp3-TEVp (or the control AAV5-EF1a-DIO-mCherry) was bilaterally injected in the striatum (500 nl/side; AP +0.80, ML ± 1.75, DV −2.75) of heterozygous ChAT-cre or ChAt-tdT mice. Four weeks later, manually-constructed optic fibers with high numerical aperture (NA; 0.66) fiber (Prizmatix) were bilaterally implanted in the DS (AP +0.80, ML ± 1.75, DV −2.25) and secured with TitanBond (Horizon) and dental cement. Animals recovered for at least one week prior to behavioral testing.

For *in vivo* photometry, DAT-cre mice were unilaterally injected with AAV5-hSyn-GCaMP6f-FLEX in the substantia nigra at a volume of 450nl at two sites (AP −3.5, ML 1.5, DV −4.75 and AP −3.0, ML 1.5, DV −4.8). These mice also received bilateral injections of AAV8-hSyn-hM4Di-mCherry or control AAV8-hSyn-mCherry in the rILN (as described above). These mice were unilaterally implanted with a low NA (0.22) fiber (ThorLabs) in the DS.

Immunohistochemistry was used to confirm virus expression at injection sites; animals were excluded from experiments for poor virus expression at targeted regions or if virus expression was detected in the Pf for rILN-targeted injections (or rILN-localized expression for Pf-targeted injections).

Brain Slice Preparation—Mice were deeply anesthetized with isoflurane and brains were quickly removed and submerged in 95% oxygen, 5% carbon dioxide (carbogen)-bubbled ice cold cutting solution (in mM): 194 sucrose, 30 NaCl, 4.5 KCl, 1 MgCl2, 26 NaHCO3, 1.2 NaH2PO4, and 10 D-glucose). 250 μm coronal slices were obtained on a Leica VT 1200 vibratome and stored in carbogen-bubbled aCSF (in mM); 124 NaCl, 4.5 KCl, 2 CaCl2, 1 MgCl2, 26 NaHCO3, 1.2 NaH2PO4, and 10 D-glucose). Striatal slices were incubated at 32.4°C for 30 min and stored thereafter at room temperature until recording.

Whole-cell Electrophysiology—Hemisected ChAT-tdTomato brain slices were transferred to the recording chamber and perfused with carbogen-bubbled aCSF (in mM; 124 NaCl, 4.5 KCl, 2 CaCl2, 1 MgCl2, 26 NaHCO3, 1.2 NaH2PO4, and 10 D-glucose) at 29-31°C. Whole-cell recordings were made with glass micropipettes (2-5 mΩ) filled with $CsMeSO_3$-based internal solution (in mM; 120 $CsMeSO_3$, 5 NaCl, 10 TEA-Cl, 10 HEPES, 5 QX-314, 1.1 EGTA, 4 Mg-ATP, and 0.3 Na-GTP; 290-300 mOsm and pH 7.3) to record oPSCs were evoked with 2-4 ms 473 nm light pulses and recorded in whole-cell voltage clamp. Drugs dissolved in aCSF were delivered to brain slices through a gravity perfusion system. Visually-identified tdTomato-expressing cholinergic interneurons were voltage-clamped at −60 mV with a MultiClamp 700B amplifier (Molecular Devices) and recordings were filtered and digitized at 2 and 10 kHz, respectively. For burst-pause experiments, cholinergic interneurons were recorded in cell-attached or whole cell current-clamp configurations with a K^+-based internal solution (in mM: 126 potassium gluconate, 4 KCl, 10 HEPES, 4 ATP-Mg, 0.3 GTP-Na, and 10 phosphocreatine; 290-295 mOsm; pH 7.3). Data was acquired with Clampex 10.4.1.4 and analyzed with Clampfit 10.4.1.4 (Molecular Devices). Cells were discarded from analysis if series resistance changed by more than 15% during recording. For voltage-clamp experiments, oPSC amplitudes were averaged per min and expressed as a percent change from baseline measurements (first 5 min of recordings). The averaged baseline was statistically compared with averaged last 5 min of recording.

FSCV—Hemisected brain slices were transferred to the recording chamber and perfused with carbogen-bubbled Krebs buffer (in nM: 126 NaCl, 2.5 KCl, 1.2 NaH2PO4, 2.4 CaCl2, 1.2 MgCl2, 0.4 L-ascorbic acid, 20 HEPES, 10 D-glucose, 25 NaHCO3, and 10 NaOH; pH 7.3 – 7.4) at 28-30°C. A 7 μm carbon fiber was aspirated into a borosilicate glass capillary tube and pulled on a P-80 horizontal pipette puller (Sutter Instruments). The extended electrode fiber was trimmed to approximately 100 μm. Voltammetry recordings and analysis were performed with TarHeel CV software (University of North Carolina). The electrode potential was linearly scanned as a triangular waveform from −0.4 to 1.3 to −0.4 V (Ag versus AgCl) at 400 V/s. Electrodes were first conditioned by applying the voltage ramp at 60 Hz for 10 min and then 10 Hz for 5 min. DA release was evoked by an optic fiber that delivered a 4 ms pulse of 10 mW blue light (473 nm) every 4 min. The first 5 stable recordings (within ± 20% nA of average) were averaged as baseline with subsequent recordings expressed as percent change of baseline measurements. Drugs dissolved in Krebs buffer were perfused immediately following the 5^{th} baseline recording for 10 subsequent recordings. Averaged baseline currents were compared with averaged recordings from the last five recordings. Due to the fleeting responses when activating Pf afferents, the first two recordings were averaged as baseline, with drugs perfused immediately following the second

recording. After a 16 min perfusion period, two additional recordings were collected and averaged. Following recording, electrodes were calibrated with 500-1000 nM DA dissolved in Krebs buffer using a microfluidic flow cell (Sinkala et al., 2012).

Behavioral Experiments—All testing was performed during the light phase, following 2-3 sessions of 15 min exposure to testing chambers.

oICSS—Food-restricted animals (90% of *ad libitum* body weight) expressing ChR2-eYFP or eYFP in the rILN were trained to lever press in a 21.6 × 17.8 × 12.7 cm operant chamber containing two retractable levers separated by a trough pellet receptacle. Pressing on either lever was reinforced with a 14 mg purified sucrose pellet (Bio-Serv) delivered on a fixed rate of one pellet per press (FR1). Mice were trained in twice-daily 30 min sessions. Once trained to lever press at least 30 times per session for 6 consecutive sessions, mice completed a single 30 min oICSS session (Day 1) in which a press on the non-biased lever (as determined from training sessions) initiated bilateral delivery of 5 Hz light for 1 s to the DS (Figure 4A). 24 hr later, light activation was paired with the opposite lever in a second oICSS session (Day 2). To test the role of DA D1 receptor signaling in rILN oICSS, mice were injected with either 0.055 mg/kg SCH23390 dissolved in 0.9% NaCl (SCH) or vehicle (Veh; 10 ml/kg *i.p.*) 30 min prior to both Day 1 and 2 test sessions. To assess the effect of drug injection (SCH or Veh) alone on motor performance, mice also completed the 2-day oICSS protocol in which presses on neither lever delivered light (No Light). Thus, each animal completed four counter-balanced oICSS tests (Veh+Light, SCH+Light, Veh+No Light, and SCH+No Light) separated by 6 FR1 food-reinforced sessions. Patch cables, connected to a commutator and 465 nm LED module (Plexon), were attached to optic fiber implants via ceramic sleeves (Thorlabs).

Open Field Assay—Mice expressing GCaMP6f in substantia nigra DA neurons and hM4Di-mCherry or mCherry alone in rILN were assessed for movement-related nigrostriatal DA terminal activity in an open arena (70 × 30 × 25 cm). Mice were injected with vehicle solution (Veh; 0.9% NaCl, 10 ml/kg *i.p.*) 40 min prior to testing. 24 hr later, mice were administered CNO (5 mg/kg *i.p.*) 40 min prior to a second open field test. Mice were video recorded for movement analysis using Ethovision XT.

Fiber Photometry—Time-correlated single-photon counting fiber photometry (TCSPC; White et al., 2018) was used to record activity-dependent calcium signals of dopaminergic nigrostriatal terminals. 20 MHz-pulsed blue light emitted from a 473-nm picosecond diode laser (Becker & Hickl) was transmitted into a multimode fiber patchcord (RJPSL2; Thorlabs) attached to a chronic fiber implant in the DS. GCaMP6f emission photons were band-pass filtered, and transmitted into a 16-channel, 106 nm wavelength photomultiplier tube (PML-16-1-C; Becker & Hickl). Photons per channel were recorded with a TCSPC module (SPC-130-EM; Becker & Hickl). The “peak signal” was derived from the photon counts from the spectral channel corresponding to maximum GCaMP6f emission following subtraction of photons from a non-GCaMP6f -related channel.

Immunohistochemistry—Mice were transcardially perfused with room-temperature 0.1 M Phosphate Buffered Saline (PBS), pH 7.3, followed by ice-cold 4% (w/v)

paraformaldehyde in PBS. Brains were extracted and post-fixed with 4% paraformaldehyde in PBS at 4°C. 50 μm coronal sections were cut using an Integraslice 7550 MM vibrating microtome (Campden Instruments). Chicken or goat anti-GFP and chicken anti-mCherry antibodies were used at a 1:2000 dilution. Goat anti-choline acetyltransferase antibody was used at 1:200. Secondary donkey anti-goat or anti-chicken antibodies conjugated to either Alexa 488 or 594 were used at 1:1000 dilution. The Brain BLAQ protocol (Kupferschmidt et al., 2017) was used for immunohistochemistry following FSCV and electrophysiology.

QUANTIFICATION AND STATISTICAL ANALYSIS

All statistical analyses were performed in Prism 6.01 and are reported in the Results. The specific statistical test as well as value and description of n are listed in the figure legends. Photon counts derived from the fiber photometry experiment were analyzed in RStudio 1.1.456 prior to statistical analysis.

Supplementary Material

Refer to Web version on PubMed Central for supplementary material.

ACKNOWLEDGMENTS

This work was supported by the University of Maryland Claude D. Pepper Older Americans Independence Center; National Institute on Alcohol Abuse and Alcoholism grants K22AA021414, R01AA024845 (to B.N.M.), and F31AA024683 (to M.H.P.); Whitehall Foundation grant 2014-12-68 (B.N.M.); National Institute on Drug Abuse grants R01DA022340, R01DA042595 (to J. F.C.), and F31DA047014 (to K.K.C.); and National Institute of Neurological Disorders and Stroke grant T32NS063391 (to K.K.C.).

REFERENCES

Aosaki T, Tsubokawa H, Ishida A, Watanabe K, Graybiel AM, and Kimura M. (1994). Responses of tonically active neurons in the primate's striatum undergo systematic changes during behavioral sensorimotor conditioning. J. Neurosci 14, 3969–3984. [PubMed: 8207500]

Bamford NS, Wightman RM, and Sulzer D. (2018). Dopamine's effects on corticostriatal synapses during reward-based behaviors. Neuron 97,494–510. [PubMed: 29420932]

Barter JW, Li S, Lu D, Bartholomew RA, Rossi MA, Shoemaker CT, Salas-Meza D, Gaidis E, and Yin HH (2015). Beyond reward prediction errors: the role of dopamine in movement kinematics. Front. Integr. Nuerosci 9, 39.

Berendse HW, and Groenewegen HJ (1990). Organization of the thalamostriatal projections in the rat, with special emphasis on the ventral striatum. J. Comp. Neurol 299, 187–228. [PubMed: 2172326]

Berke JD (2018). What does dopamine mean? Nat. Neurosci 21, 787–793. [PubMed: 29760524]

Bradfield LA, Bertran-Gonzalez J, Chieng B, and Balleine BW (2013). The thalamostriatal pathway and cholinergic control of goal-directed action: interlacing new with existing learning in the striatum. Neuron 79, 153–166. [PubMed: 23770257]

Cachope R, Mateo Y, Mathur BN, Irving J, Wang HL, Morales M, Lovinger DM, and Cheer JF (2012). Selective activation of cholinergic interneurons enhances accumbal phasic dopamine release: setting the tone for reward processing. Cell Rep. 2, 33–41. [PubMed: 22840394]

Chen TW, Wardill TJ, Sun Y, Pulver SR, Renninger SL, Baohan A, Schreiter ER, Kerr RA, Orger MB, Jayaraman V, et al. (2013). Ultrasensitive fluorescent proteins for imaging neuronal activity. Nature 499, 295–300. [PubMed: 23868258]

Chen CH, Fremont R, Arteaga-Bracho EE, and Khodakhah K. (2014). Short latency cerebellar modulation of the basal ganglia. Nat. Neurosci 17, 1767–1775. [PubMed: 25402853]

del Campo N, Fryer TD, Hong YT, Smith R, Brichard L, Acosta-Cabronero J, Chamberlain SR, Tait R, Izquierdo D, Regenthal R, et al. (2013). A positron emission tomography study of nigro-striatal dopaminergic mechanisms underlying attention: implications for ADHD and its treatment. Brain 136, 3252–3270. [PubMed: 24163364]

Ding JB, Guzman JN, Peterson JD, Goldberg JA, and Surmeier DJ (2010). Thalamic gating of corticostriatal signaling by cholinergic interneurons. Neuron 67, 294–307. [PubMed: 20670836]

Ellender TJ, Harwood J, Kosillo P, Capogna M, and Bolam JP (2013). Heterogeneous properties of central lateral and parafascicular thalamic synapses in the striatum. J. Physiol 591, 257–272. [PubMed: 23109111]

Fan D, Rossi MA, and Yin HH (2012). Mechanisms of action selection and timing in substantia nigra neurons. J. Neurosci 32, 5534–5548. [PubMed: 22514315]

Faure A, Haberland U, Condé F, and El Massioui N. (2005). Lesion to the nigrostriatal dopamine system disrupts stimulus-response habit formation. J. Neurosci 25, 2771–2780. [PubMed: 15772337]

Fiorillo CD, Tobler PN, and Schultz W. (2003). Discrete coding of reward dopamine neurons. Science 299, 1898–1902. [PubMed: 12649484]

Halliday GM (2009). Thalamic changes in Parkinson's disease. Parkinsonism Relat. Disord 15 (Suppl 3), S152–S155. [PubMed: 20082979]

Hamid AA, Pettibone JR, Mabrouk OS, Hetrick VL, Schmidt R, Vander Weele CM, Kennedy RT, Aragona BJ, and Berke JD (2016). Mesolimbic dopamine signals the value of work. Nat. Neurosci 19, 117–126. [PubMed: 26595651]

Hanganu A, Provost J-S, and Monchi O. (2015). Neuroimaging studies of striatum in cognition part II: Parkinson's disease. Front. Syst. Neurosci 9, 138. [PubMed: 26500512]

Howard CD, Li H, Geddes CE, and Jin X. (2017). Dynamic nigrostriatal dopamine biases action selection. Neuron 93, 1436–1450. [PubMed: 28285820]

Howe MW, and Dombeck DA (2016). Rapid signalling in distinct dopaminergic axons during locomotion and reward. Nature 535, 505–510. [PubMed: 27398617]

Howe MW, Tierney PL, Sandberg SG, Phillips PEM, and Graybiel AM (2013). Prolonged dopamine signalling in striatum signals proximity and value of distant rewards. Nature 500, 575–579. [PubMed: 23913271]

Hunnicutt BJ, Jongbloets BC, Birdsong WT, Gertz KJ, Zhong H, and Mao T. (2016). A comprehensive excitatory input map of the striatum reveals novel functional organization. eLife 5, 1–33.

Jin X, and Costa RM (2010). Start/stop signals emerge in nigrostriatal circuits during sequence learning. Nature 466, 457–462. [PubMed: 20651684]

Kato S, Fukabori R, Nishizawa K, Okada K, Yoshioka N, Sugawara M, Maejima Y, Shimomura K, Okamoto M, Eifuku S, and Kobayashi K. (2018). Action selection and flexible switching controlled by the intralaminar thalamic neurons. Cell Rep. 22, 2370–2382. [PubMed: 29490273]

Kosillo P, Zhang Y-F, Threlfell S, and Cragg SJ (2016). Cortical control of striatal dopamine transmission via striatal cholinergic interneurons. Cereb. Cortex 26, 4160–4169.

Kupferschmidt DA, Juczewski K, Cui G, Johnson KA, and Lovinger DM (2017). Parallel, but dissociable, processing in discrete corticostriatal inputs encodes skill learning. Neuron 96, 476–489. [PubMed: 29024667]

Lacey CJ, Bolam JP, and Magill PJ (2007). Novel and distinct operational principles of intralaminar thalamic neurons and their striatal projections. J. Neurosci 27, 4374–4384. [PubMed: 17442822]

Li X, Witonsky KR, Lofaro OM, Surjono F, Zhang J, Bossert JM, and Shaham Y. (2018). Role of anterior intralaminar nuclei of thalamus projections to dorsomedial striatum in incubation of methamphetamine craving. J. Neurosci 38, 2270–2282. [PubMed: 29371321]

Mateo Y, Johnson KA, Covey DP, Atwood BK, Wang H-L, Zhang S, Gildish I, Cachope R, Bellocchio L, Guzman M, et al. (2017). Endocannabinoid actions on cortical terminals orchestrate local modulation of dopamine release in the nucleus accumbens. Neuron 96, 1112–1126. [PubMed: 29216450]

Matsuda W, Furuta T, Nakamura KC, Hioki H, Fujiyama F, Arai R, and Kaneko T. (2009). Single nigrostriatal dopaminergic neurons form widely spread and highly dense axonal arborizations in the neostriatum. J. Neurosci 29, 444–453. [PubMed: 19144844]

Melief EJ, McKinley JW, Lam JY, Whiteley NM, Gibson AW, Neumaier JF, Henschen CW, Palmiter RD, Bamford NS, and Darvas M. (2018). Loss of glutamate signaling from the thalamus to dorsal striatum impairs motor function and slows the execution of learned behaviors. NPJ Parkinsons Dis. 4, 23. [PubMed: 30083593]

Parker NF, Cameron CM, Taliaferro JP, Lee J, Choi JY, Davidson TJ, Daw ND, and Witten IB (2016). Reward and choice encoding in terminals of midbrain dopamine neurons depends on striatal target. Nat. Neurosci 19, 845–854. [PubMed: 27110917]

Pissadaki EK, and Bolam JP (2013). The energy cost of action potential propagation in dopamine neurons: clues to susceptibility in Parkinson's disease. Front. Comput. Neurosci 7, 13. [PubMed: 23515615]

Renfroe JB, Bradley MM, Okun MS, and Bowers D. (2016). Motivational engagement in Parkinson's disease: Preparation for motivated action. Int. J. Psychophysiol 99, 24–32. [PubMed: 26659013]

Robinson S, Rainwater AJ, Hnasko TS, and Palmiter RD (2007). Viral restoration of dopamine signaling to the dorsal striatum restores instrumental conditioning to dopamine-deficient mice. Psychopharmacology (Berl.) 191, 567–578. [PubMed: 17093978]

Roitman MF, Stuber GD, Phillips PE, Wightman RM, and Carelli RM (2004). Dopamine operates as a subsecond modulator of food seeking. J. Neurosci. 24, 1265–1271. [PubMed: 14960596]

Schultz W (2001). Reward signaling by dopamine neurons. Neuroscientist 7, 293–302. [PubMed: 11488395]

Sinkala E, McCutcheon JE, Schuck MJ, Schmidt E, Roitman MF, and Eddington DT (2012). Electrode calibration with a microfluidic flow cell for fast-scan cyclic voltammetry. Lab Chip 12, 2403–2408. [PubMed: 22522908]

Smith Y, Galvan A, Ellender TJ, Doig N, Villalba RM, Huerta-Ocampo I, Wichmann T, and Bolam JP (2014). The thalamostriatal system in normal and diseased states. Front. Syst. Neurosci 8, 5. [PubMed: 24523677]

Soghomonian JJ, Descarries L, and Watkins KC (1989). Serotonin innervation in adult rat neostriatum. II. Ultrastructural features: a radioautographic and immunocytochemical study. Brain Res. 481, 67–86. [PubMed: 2706468]

Threlfell S, Lalic T, Platt NJ, Jennings KA, Deisseroth K, and Cragg SJ (2012). Striatal dopamine release is triggered by synchronized activity in cholinergic interneurons. Neuron 75, 58–64. [PubMed: 22794260]

Van der Werf YD, Witter MP, and Groenewegen HJ (2002). The intralaminar and midline nuclei of the thalamus. Anatomical and functional evidence for participation in processes of arousal and awareness. Brain Res. Brain Res. Rev 39, 107–140. [PubMed: 12423763]

Volkow ND, Wang G-J, Newcorn J, Telang F, Solanto MV, Fowler JS, Logan J, Ma Y, Schulz K, Pradhan K, et al. (2007a). Depressed dopamine activity in caudate and preliminary evidence of limbic involvement in adults with attention-deficit/hyperactivity disorder. Arch. Gen. Psychiatry 64, 932–940. [PubMed: 17679638]

Volkow ND, Fowler JS, Wang G-J, Swanson JM, and Telang F (2007b). Dopamine in drug abuse and addiction: results of imaging studies and treatment implications. Arch. Neurol 64, 1575–1579. [PubMed: 17998440]

White MG, Panicker M, Mu C, Carter AM, Roberts BM, Dharmasri PA, and Mathur BN (2018). Anterior cingulate cortex input to the claustrum is required for top-down action control. Cell Rep. 22, 84–95. [PubMed: 29298436]

Wichmann T, and DeLong MR (2003). Pathophysiology of Parkinson's disease: the MPTP primate model of the human disorder. Ann. NY Acad. Sci 991, 199–213. [PubMed: 12846988]

Zhang Y-F, Reynolds JNJ, and Cragg SJ (2018). Pauses in cholinergic interneuron activity are driven by excitatory input and delayed rectification, with dopamine modulation. Neuron 98, 918–925 [PubMed: 29754751]

Highlights

- The rostral intralaminar nuclei of the thalamus (rILN) project to the dorsal striatum
- Glutamatergic rILN projections induce local dopamine release in the dorsal striatum
- rILN activity suppression correlates with reduced nigrostriatal activity and movement
- rILN terminal activation supports behavioral reinforcement

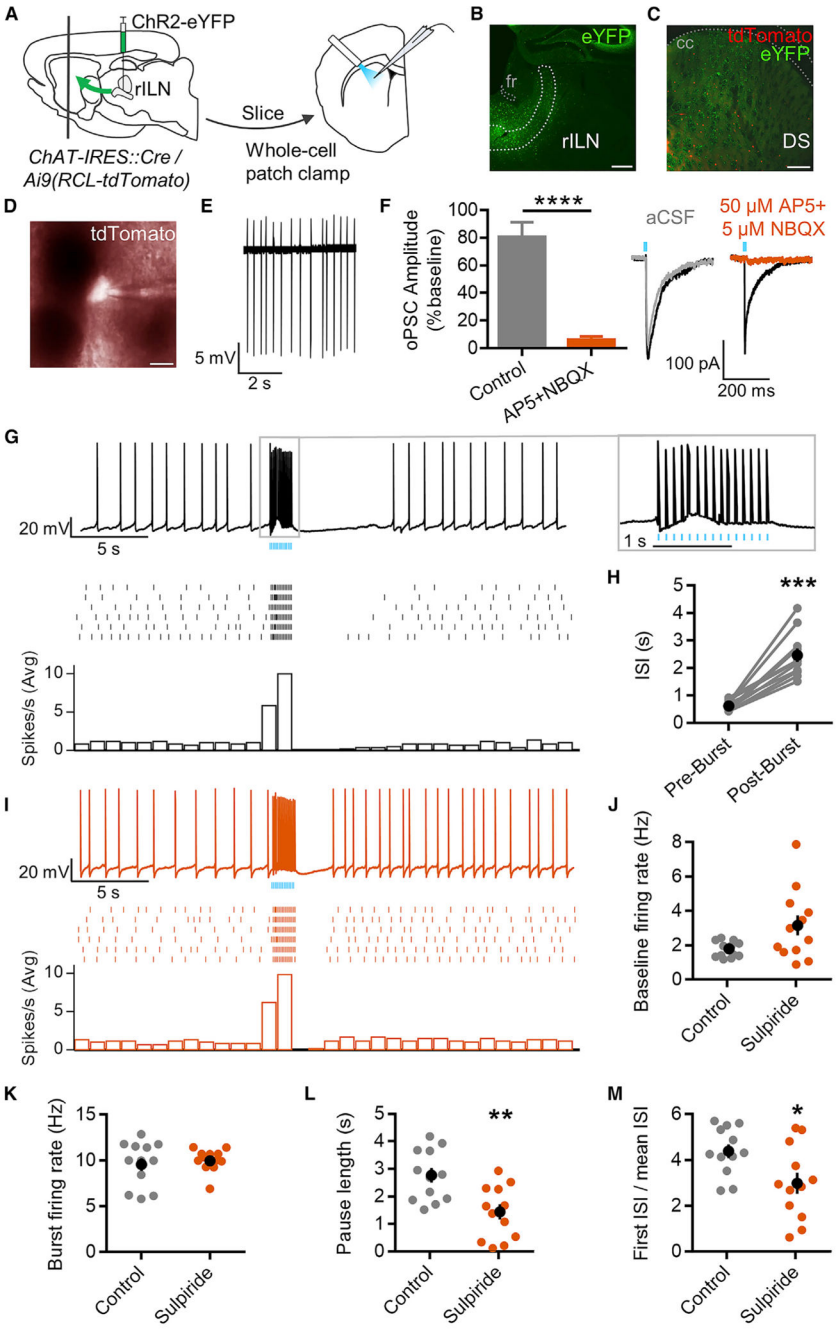

Figure 1. Thalamic rILN Activate Striatal Cholinergic Interneurons

(A) Schematic of experimental approach.

(B) Representative expression of channelrhodopsin (ChR2)-eYFP at the rostral intralaminar nuclei of the thalamus (rILN) injection site.

(C) Representative expression of ChR2-eYFP in rILN axon terminals (green) and cholinergic interneurons (red) in the dorsal striatum (DS).

(D) Recorded tdTomato-expressing cholinergic interneuron.

(E) Sample trace of a cell-attached cholinergic interneuron recording.

(F) Left: NBQX and AP5 application reduced the average peak amplitude of post-synaptic currents evoked by optogenetic activation (oPSCs; one 2–4 ms pulse, blue bar) of ChR2-expressing rILN terminals (orange; n = 6 cells) versus control aCSF (gray; n = 4 cells). Right: representative oPSCs: control (black), after incubation in aCSF (gray), or NBQX and AP5 (orange).

(G) Top: representative whole-cell current-clamp recording of burst firing in a cholinergic interneuron in response to optogenetic rILN terminal activation (15 pulses at 10 Hz), followed by a firing pause. Middle: representative raster plots of six consecutive responses. Bottom: corresponding histogram of average firing per second.

(H) Time to first spike following burst firing was greater than the average interspike interval (ISI) during tonic firing (n = 11 cells).

(I) Representative cholinergic interneuron recording following incubation in 5 μM sulpiride (top), with a raster plot of six consecutive responses (middle) and corresponding histogram (bottom).

(J–M) Comparison of cholinergic interneuron burst-pause firing properties between control (n = 12 cells) and in sulpiride (n = 12 cells) of (J) baseline firing rate, (K) burst firing rate, (L) post-burst-pause length, and (M) ratio of post-burst ISI to mean baseline ISI.

aCSF, artificial cerebral spinal fluid; cc, corpus callosum; fr, fasciculus retroflexus. Scale bars: 250 μm (B and C) and 40 μm (D). Unpaired t test (F); Wilcoxon signed-rank test (H); Mann-Whitney test (J–M): *p < 0.05, **p < 0.01, ***p < 0.001, ****p < 0.0001. Individual values are represented in gray or orange, with mean ± SEM in black.

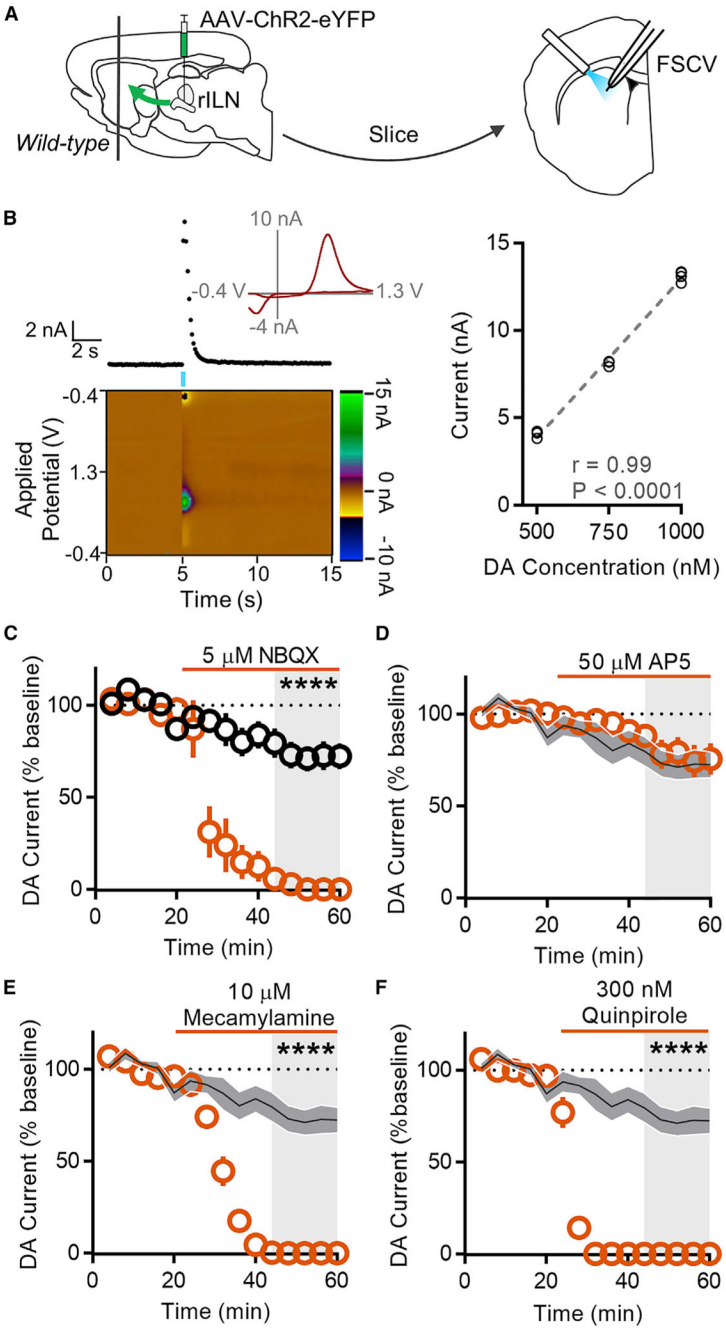

Figure 2. rILN Afferent Activation Evokes DA Release in the DS

(A) Approach for fast-scan cyclic voltammetry (FSCV) recordings.

(B) Left: optogenetic rILN terminal activation in the DS elicited a dopamine (DA) current with a corresponding cyclic voltammogram (top) and a plot of the background-subtracted current (bottom). Right: representative electrode calibration of the current to known DA concentrations (3–4 recordings per concentration).

(C) DA release time course in control (black; n = 8 recordings) and following NBQX application (orange; n = 8 slices).

(D) AP5 (orange) did not alter rILN-induced DA release (n = 8 slices).

(E) Mecamylamine (orange) abolished DA release (n = 8 slices).
(F) Quinpirole (orange) eliminated DA release (n = 7 slices).
Unpaired t test (C–F): ****$p < 0.0001$. Data represent mean ± SEM.

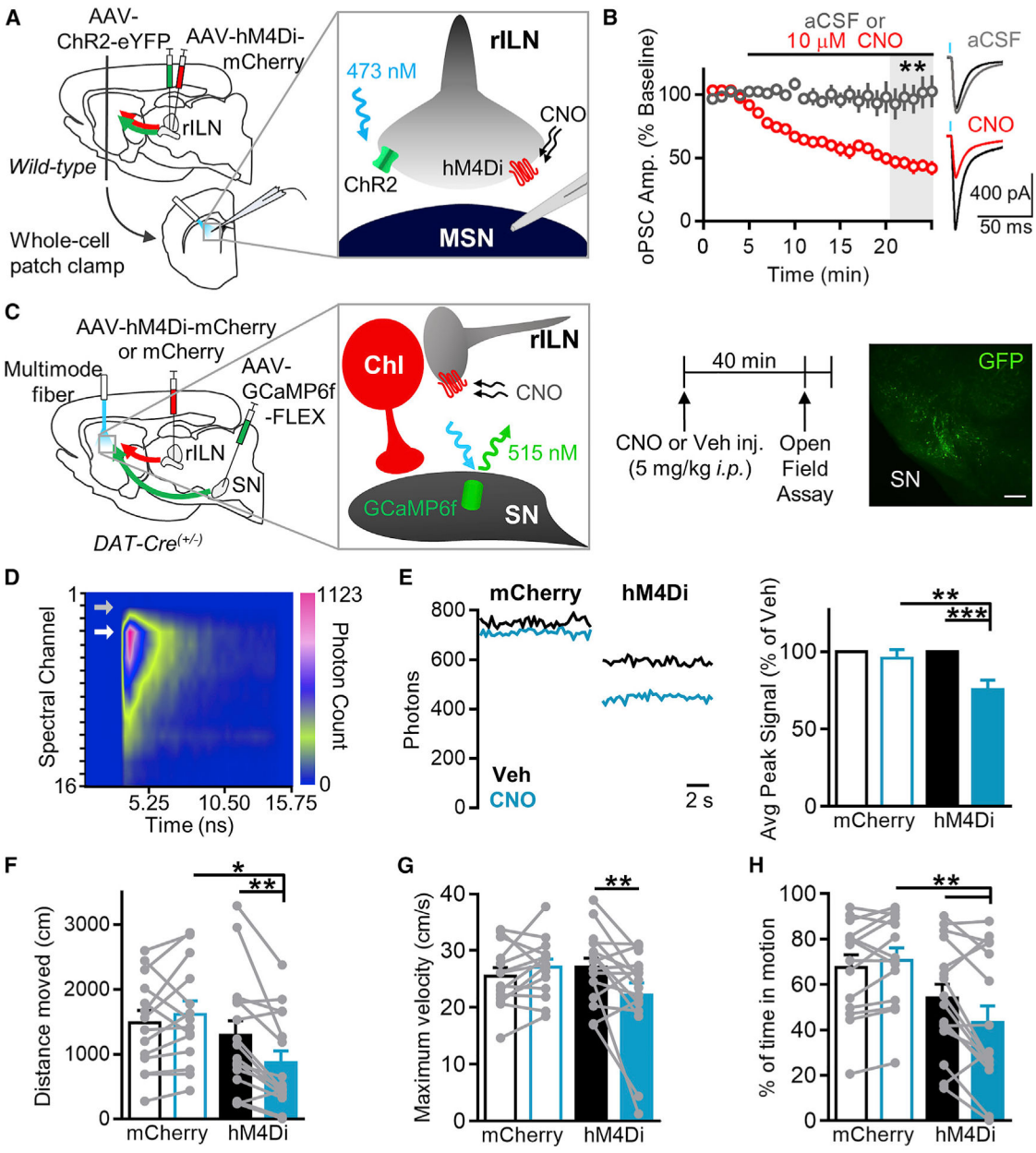

Figure 3. Chemogenetic Suppression of rILN Firing Decreases Dopaminergic Nigrostriatal Terminal Activity and Locomotion

(A) Approach for chemogenetic rILN terminal inhibition and synaptic transmission interrogation.

(B) Left: recording from DS medium spiny neurons (MSNs) in striatal slices; application of clozapine-N-oxide (CNO; red) attenuated rILN-evoked oPSC amplitude (n = 6 cells) as compared to control aCSF (gray; n = 9 cells). Right: representative oPSC traces, before (black) and after aCSF (gray) or CNO (red) incubation.

(C) Left: experimental strategy to chemogenetically suppress rILN activity and monitor dopaminergic nigrostriatal terminal activity. Middle: timeline of drug administration and

behavioral testing. Right: representative expression of GCaMP6f (green) in the substantia nigra (SN).

(D) Emission profile of GCaMP6f in the DS, with the peak GCaMP6f channel (white arrow) and off-peak channel (gray arrow).

(E) Left: representative traces of the peak signal in hM4Di and mCherry-expressing mice moving freely in an open field following vehicle (Veh; black) or CNO (blue; 5 mg/kg) injection. Right: average peak signal was decreased in hM4Di-expressing mice (N = 16 mice), but not mCherry-expressing mice (N = 14 mice), by CNO.

(F–H) Changes in movement between groups: (F) total distance traveled, (G) maximum velocity, and (H) percentage of time in motion.

Scale bar: 250 μm. Unpaired t test (B); post hoc Holm-Šidàk test (E–H): *$p < 0.05$, **$p < 0.01$, ***$p < 0.001$. Individual values are represented in gray; data represent mean ± SEM.

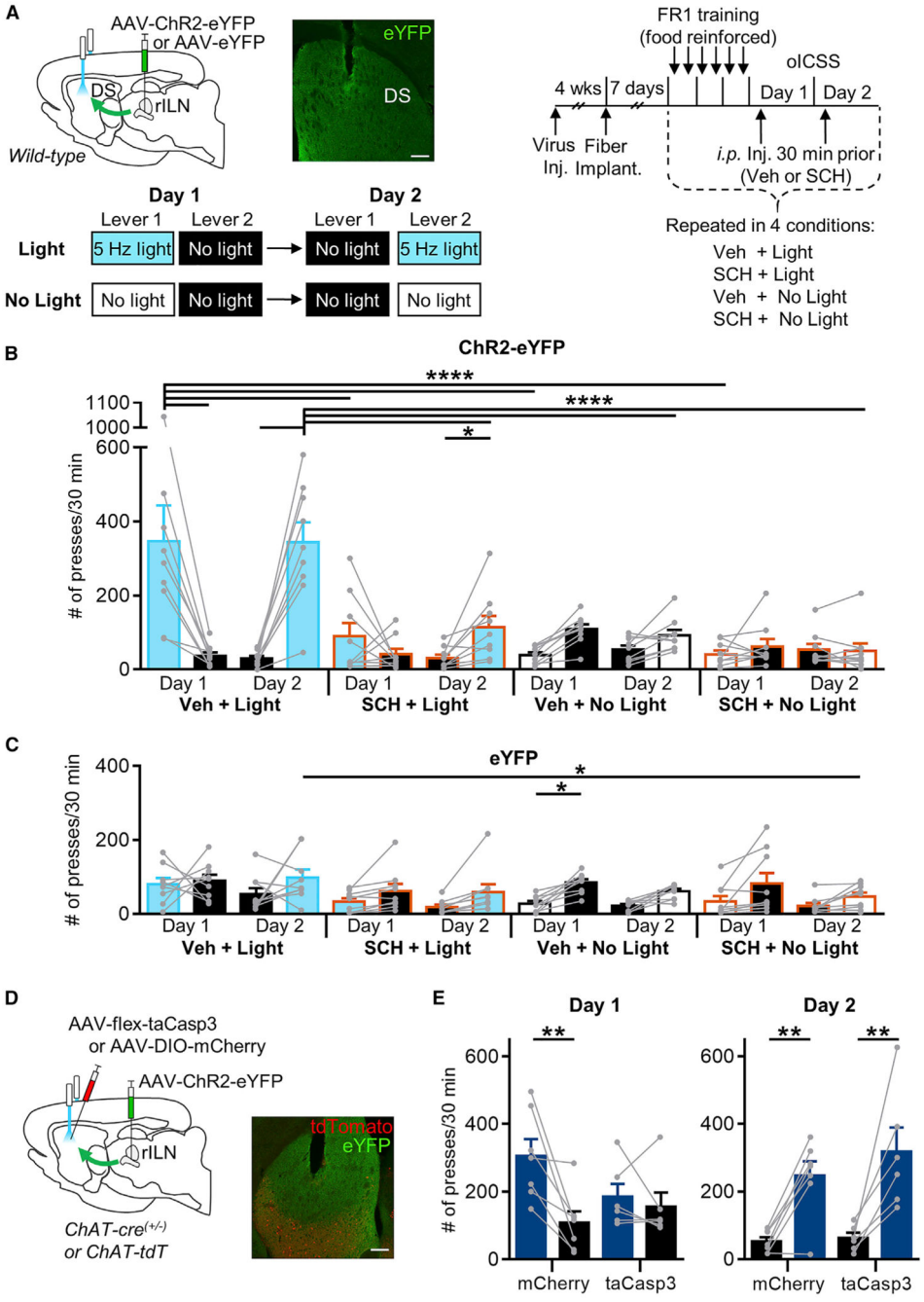

Figure 4. Optogenetic Activation of rILN Afferents in the DS Is Reinforcing

(A) Top left: approach for *in vivo* optogenetic rILN-terminal activation and ChR2-eYFP expression relative to fiber placement in DS. Right and bottom left: experimental timeline and procedure for a two-day optical intracranial self-stimulation paradigm (oICSS).

(B) ChR2-eYFP-expressing mice pressed the light-paired lever (blue fill) more than the non-reinforced lever (black fill) in a light and DA D1 receptor-dependent manner.

(C) eYFP-expressing mice did not press the light-paired lever more than the non-reinforced lever (N = 9 mice).

(D) Left: strategy to ablate DS cholinergic interneurons at site of light delivery. Right: representative taCasp3-mediated ablation of cholinergic interneurons (red) and expression of ChR2-eYFP-expressing rILN terminals (green) in the DS.

(E) mCherry-expressing mice (N = 7) pressed the light-paired lever (blue) more than the non-reinforced lever (black) on both test days. taCasp3-ablated mice (N = 6) only pressed the light-paired lever more on day 2.

FR1, fixed-rate 1; SCH, SCH23390. Scale bars = 250 μm. Post hoc Holm-Šidàk test: *$p < 0.05$, **$p < 0.01$, ****$p < 0.0001$. Individual values are represented in gray; data represent mean ± SEM.

See also Figure S2.

KEY RESOURCES TABLE

Reagent or Resource	Source	Identifier
Antibodies		
Chicken anti-GFP	Abcam	#ab13970;RRID:AB_300798
Goat anti-GFP	Abcam	#ab6673; RRID:AB_305643
Chicken anti-mCherry	Novus Biologicals	#NBP2-25158; RRID:AB_2636881
Alexa 488 Donkey anti-Goat	Jackson ImmunoResearch	#705-545-003; RRID:AB_2340428
Alexa 488 Donkey anti-Chicken	Jackson ImmunoResearch	#703-545-155; RRID:AB_2340375
Alexa 594 Donkey anti-Goat	Jackson ImmunoResearch	#705-585-147; RRID:AB_2340433
Alexa 594 Donkey anti-Chicken	Jackson ImmunoResearch	#703-585-155; RRID:AB_2340377
Goat anti-Choline Acetyltransferase	Novus Biologicals	#NBP1-30052; RRID:AB_1968484
Bacterial and Virus Strains		
AAV5-hSyn-hChR2(H134R)-eYFP	Karl Deisseroth / Addgene	26973-AAV5
AAV5-hSyn-eYFP	Karl Deisseroth / UNC Vector Core	N/A
AAV5-hSyn-GCaMP6f-FLEX	Chen et al., 2013 / Addgene	100833-AAV5
AAV8-hSyn-hM4Di-mCherry	Bryan Roth / Duke Viral Vector Core	N/A
AAV5-flex-taCasp3-TEVp	Nirao Shah / UNC Vector Core	N/A
AAV5-EF1a-DIO-mCherry	Karl Deisseroth / UNC Vector Core	N/A
AAV8-hSyn-mCherry	Karl Deisseroth / UNC Vector Core	N/A
Chemicals, Peptides, and Recombinant Proteins		
Clozapine-N-oxide	Abcam	#ab141704
DL-AP5 sodium salt	Abcam	#ab120271
Mecamylamine hydrochloride	Tocris Bioscience	#2843
NBQX disodium salt	Abcam	#ab120046
(−)-Quinpirole hydrochloride	Tocris Bioscience	#1061
R(+)-SCH23390 hydrochloride	Sigma-Aldrich	#D054
(RS)-(±)-Sulpiride	Tocris Bioscience	#0894
Experimental Models: Organisms/Strains		
Mouse, C57BL/6J	Jackson Laboratory	#000664
Mouse, ChAT-IRES-Cre	Jackson Laboratory	#028861
Mouse, Ai9(RCL-tdT)	Jackson Laboratory	#007909
Mouse, DAT-IRES-Cre	Jackson Laboratory	#006660
Software and Algorithms		
Data analysis: Prism 6.01	Graphpad	https://www.graphpad.com/
Data analysis: RStudio 1.1.456	RStudio	https://www.rstudio.com/
MedPC-IV 4.2	Med Associates	SOF-735
Ethovision XT v11.5	Noldus	https://www.noldus.com/
Other		
Operant Chamber	Med Associates	ENV-307W